The Cryosphere Discuss., https://doi.org/10.5194/tc-2018-60
Manuscript under review for journal The Cryosphere
Discussion started: 6 April 2018

The Cryosphere Discussions
Open Access
EGU

Attribution of sea ice model biases to specific model errors enabled by new induced surface flux framework

Alex West[1], Mat Collins[2], Ed Blockley[1], Jeff Ridley[1], Alejandro Bodas-Salcedo[1]

[1]Met Office Hadley Centre, FitzRoy Road, Exeter, EX1 3PB
[2]Centre for Engineering, Mathematics and Physical Sciences, University of Exeter, Exeter, EX4 4SB, UK

Correspondence to: Alex E. West (alex.west@metoffice.gov.uk)

Abstract. A new framework is presented for analysing the causes of model sea ice biases, demonstrated with the CMIP5 model HadGEM2-ES. Arctic sea ice extent has decreased over recent decades and has reached historic minima in late summer in recent years. Climate models project an ice-free Arctic in late summer during the 21st century, with wide-ranging implications for global climate and geopolitics. However, substantial spread remains in climate model projections of the rate of sea ice decline, with drivers poorly understood. In the framework described, the sea ice volume is treated as a consequence of the integrated surface energy balance. A system of simple models allows specific portions of the surface flux anomaly to be attributed to individual processes by calculating for each process an 'induced surface flux anomaly'. The method allows detailed quantification of the role played by the surface albedo and ice thickness-growth feedbacks in causing anomalous sea ice melt and growth. It shows biases in the HadGEM2-ES sea ice volume simulation to be due to a bias in spring surface melt onset date, partly countered by a counteracting bias in winter downwelling longwave radiation. The framework is applicable in principle to any model and has the potential to greatly improve understanding of the reasons for ensemble spread in modelled sea ice state.

1. Introduction

The Arctic sea ice cover has witnessed rapid change during the past 30 years, most notably with a decline in September extent of 1.05 x 10^6 km^2 / decade from 1986-2015 (HadISST1.2, Rayner et al 2003). In association with the changes in extent, evidence of declining Arctic sea ice thickness has been observed from submarine and satellite data (Rothrock et al, 2008, Lindsay and Schweiger, 2015). Arctic sea ice is also thought to have become younger on average as reserves of older ice have been lost (Maslanik et al, 2011), and the beginning of summer melt onset has been observed to become earlier in the year (Markus et al, 2009).

The changes have focussed much interest on model projections of Arctic sea ice, whoseloss influences the climate directly through increased absorption of shortwave (SW) radiation during summer and through greater release of heat from the ocean to the atmosphere during winter (Stroeve et al, 2012b). However, substantial spread remains in model simulations of present-day Arctic sea ice, and of the long-term rate of decline under climate change (Stroeve et al, 2012a). The causes of this spread are at present poorly understood, resulting in considerable uncertainty in future projections of Arctic sea ice.

Evaluating sea ice extent or volume with respect to observations shows that some models clearly reproduce present-day sea ice state more accurately than others (e.g. Wang and Overland, 2012; Massonet et al, 2012; Shu et al, 2015). However, an accurate simulation of sea ice extent and volume under the present-day climate does not necessarily imply an accurate future projection of sea ice change, as a correct simulation can be obtained by accident due to cancelling model errors, or internal variability. Sea ice extent in particular is known to be a very unsuitable metric for diagnosing model performance due to its very high internal variability (Notz, 2015; Swart et al, 2015). Hence there is a need to better understand the drivers which lead a model to simulate a given Arctic sea ice state.

Ice volume is, to first order, proportional to the heat required to melt the ice, and therefore acts to integrate the surface and basal energy balance. Basal melting in the interior ice pack has been shown to derive in the main from direct solar heating of the ocean (e.g Maykut and McPhee, 1995), while basal freezing derives principally from conduction of energy upward through the ice (Perovich and Elder, 2002); this implies that the surface energy balance (SEB) contains the principal sources and sinks of energy for the sea ice on an Arctic-wide scale. However, a complex two-way relationship exists between sea ice thickness and surface energy balance, via the surface temperature and surface albedo, giving rise to the thickness-growth feedback (Bitz and Roe, 2004) and the surface albedo feedback (Bitz, 2008), both of which exert first-order control on the sea ice state. Hence many components of the SEB cannot be viewed as independent of the sea ice state in any meaningful sense.

This study, which presents a new framework to investigate the causes of modelled sea ice anomalies, is motivated by a desire to separate, to first order, many external drivers of the SEB (and hence the sea ice state) from the thickness-growth and albedo feedbacks, and thereby understand the processes that result in a particular modelled sea ice state being simulated. The analysis uses as a case study a member of the historical ensemble of the coupled model HadGEM2-ES, a CMIP5 model which simulates anomalously low annual minimum ice extent, and which simulates an ice volume which is both too low in the annual mean and too amplified in the seasonal cycle, a similar behaviour to that identified by Shu et al (2015) in the CMIP5 ensemble mean.

In the framework presented, the principal components of the SEB, shortwave and longwave radiative fluxes, are expressed in terms of key Arctic climate variables using two simple models, for the freezing and melting seasons respectively. With the use of the simple models, and reference datasets for the climate variables, the model anomaly in surface flux induced by each climate variable can be estimated. In this way, anomalies in ice growth and melt over the course of the year are attributed via the SEB to biases in specific model quantities. The method allows the contributions to model anomalies in ice growth and melt of the sea ice albedo feedback, the ice thickness-growth feedback, and of various external factors, to be separately quantified. In this way it can be seen how model biases in the external drivers are able to produce a particular sea ice state, offering a valuable tool for setting sea ice state biases in context, and for understanding spread in sea ice simulation within multimodel ensembles.

In Section 2, the HadGEM2-ES model and the observational datasets used are described in turn, and the induced surface flux method is introduced. In Section 3 the sea ice and surface radiation simulations of HadGEM2-ES are evaluated. In Section 4 the induced surface flux analysis is applied to HadGEM2-ES, allowing quantification of the role played by anomalies in specific Arctic climate variables in causing anomalous ice growth and melt.

The Cryosphere Discuss., https://doi.org/10.5194/tc-2018-60
Manuscript under review for journal The Cryosphere
Discussion started: 6 April 2018

In Section 5 the implications of the results are discussed, in particular the mechanisms by which the external drivers identified cause the modelled sea ice state, and the likely drivers behind the corresponding model biases. Conclusions are presented in Section 6.

2. Data and methods

2.1 The HadGEM2-ES model

HadGEM2-ES is a coupled climate model employing additional components to simulate terrestrial and oceanic ecosystems, and tropospheric chemistry (Collins et al, 2011). It is part of the 'HadGEM2' family, a collection of models that all use the HadGEM2-AO coupled atmosphere-ocean system. HadGEM2-AO is developed from HadGEM1 (Johns et al, 2006), a coupled atmosphere-ocean model whose sea ice extent simulation was recognised as being among the closest to observations out of the CMIP3 ensemble models (Wang and Overland, 2009). While the atmospheric and ocean components of HadGEM2-ES contain a large number of improvements relative to HadGEM1, many of these targeted at improving simulations of tropical weather, the sea ice component is very similar to that of HadGEM1 except for three minor modifications (Martin et al, 2011, table A4).

The sea ice component of HadGEM2-ES includes a sub gridscale sea ice thickness distribution (Thorndike et al, 1975), elastic-viscous-plastic sea ice dynamics (Hunke and Dukowicz, 1997) and incremental remapping (Lipscomb and Hunke, 2004). The thermodynamic component is a zero-layer model, with no heat capacity, described in the appendix of Semtner (1976). Most processes are calculated in the ocean model, but the SEB calculations are carried out in the atmosphere model, which passes top melting flux and conductive heat flux to the ocean model as forcing for the remaining components. A more complete description of this component can be found in McLaren et al (2006).

This study uses the first ensemble member of the 'historical' experiment of HadGEM2-ES, forced with observed solar, volcanic and anthropogenic forcing from 1860 to 2005. The period 1980-1999 is chosen for the model evaluation, as a period which predates much of the recent rapid Arctic sea ice loss, with its associated climatic changes, and which is recent enough to allow the use of a reasonable range of observational data. All analysis is carried out with data restricted to the Arctic Ocean region, shown in Figure 1.

2.2 Observational data

Uncertainty in observed variables tends to be higher in the Arctic than in many other parts of the world. There are severe practical difficulties with collecting in situ data on a large scale over regions of ice-covered ocean. While satellites have in many cases been able to produce Arctic-wide measurements of some characteristics, most notably sea ice concentration, the relative lack of in situ observations against which these can be calibrated means knowledge of the observational biases is limited. Reanalysis data over the Arctic is also more subject to the reanalysis model errors than in other regions, as there are fewer direct observations available for assimilation (Lindsay et al, 2014). The approach of this study is to use a wide range of observational data to evaluate

modelled sea ice state and surface radiative fluxes, and to use as reference datasets for the induced surface flux framework, using the small number of in situ validation studies to set results in context as far as possible.

To evaluate modelled sea ice fraction, we use the HadISST1.2 dataset (Rayner et al, 2003), derived from passive microwave observations. To evaluate modelled sea ice thickness Arctic-wide, we use the ice-ocean model PIOMAS (Schweiger et al, 2011), which is forced with the NCEP reanalysis and assimilates ice concentration data. Laxon et al (2013) and Wang et al (2016) found PIOMAS to estimate anomalously low winter ice thicknesses compared to satellite observations in some years. In particular, Wang et al (2016) found PIOMAS to have a mean bias of -0.31m relative to observations from the IceSAT satellite laser sensor. To set the PIOMAS comparison in context, we use two additional datasets to evaluate the model over smaller regions; measurements from radar altimetry aboard the ERS satellites from 1993-2000 (Laxon et al, 2003), limited to latitudes below 82°N; and estimates compiled by Rothrock et al (2008), derived from a multiple regression of submarine transects over the Central Arctic Ocean from 1975-2000, constrained to be seasonally symmetric.

To evaluate modelled surface radiative fluxes across the whole Arctic Ocean, three datasets are used. Firstly, we use the CERES-EBAF (Clouds and Earth's Radiant Energy Systems – Energy Balanced And Filled) Ed2.7 dataset (Loeb et al, 2009), based on direct measurements of top-of-atmosphere radiances from EOS sensors aboard NASA satellites, available from 2000 – present. Secondly, we use the ISCCP-FD (International Satellite Cloud Climatology Project FD-series) product, derived from the ISCCP-D cloud product described below using a radiative transfer algorithm (Zhang et al, 2004). Lastly, we use the ERA-Interim (ERAI) reanalysis dataset, which provides gridded surface flux data from 1979-present using a reanalysis system driven by the ECMWF (European Centre for Medium-range Weather Forecasts) IFS forecast model and the 4D-Var atmospheric data assimilation system (Dee et al, 2011).

To the authors' knowledge, in-situ validation of these datasets in the Arctic has been quite limited, but Christensen et al (2016) found CERES to perform quite well relative to other products, albeit underestimating downwelling LW fluxes from November – February by 10-20 Wm^{-2} relative to in situ observations at Barrow (Alaska). Liu et al (2005) found ISCCP-FD to simulate SW radiative fluxes quite accurately relative to observations from SHEBA, but to underestimate downwelling SW fluxes in spring by over 30 Wm^{-2}, also overestimating downwelling LW fluxes in winter by around 40 Wm^{-2} . Finally, Lindsay et al (2014) identified ERAI as producing a relatively accurate simulation of surface fluxes compared to in situ observations at Barrow (Alaska) and Ny-Ålesund (Svalbard), although tending to underestimate downwelling SW fluxes in the spring by up to 20 Wm^{-2} and overestimate downwelling LW fluxes in the winter by around 15 Wm^{-2}.

In addition to the datasets above, in section 4 we make use of satellite estimates of date of melt onset over sea ice (Anderson et al, 2012), also derived from passive microwave sensors; and in section 5, the CERES-SYN dataset (Rutan et al, 2015), similar to CERES-EBAF but available at higher temporal resolution, is used to examine modelled surface radiation evolution during May in more detail.

2.3 Calculating induced surface flux anomaly

The Cryosphere Discuss., https://doi.org/10.5194/tc-2018-60
Manuscript under review for journal The Cryosphere
Discussion started: 6 April 2018

Because the latent heat of sea ice is an order of magnitude greater than the sensible heat required to raise the ice to the melting temperature, ice volume is very nearly proportional to the heat required to melt the ice. Ice volume therefore acts to integrate the surface and basal energy balance, and is largely determined by the fluxes at these interfaces. Across much of the Arctic the sea ice is insulated from the main source of heat energy from beneath, the warm Atlantic water layer, by fresh water derived mainly from river runoff (e.g. Serreze et al, 2006; Stroeve et al, 2012b). Because of this, although advection-derived ocean heating can be important in setting the wintertime ice edge (Bitz et al, 2005), direct solar heating of the ocean is likely to be an order of magnitude higher in accounting for basal melting of the sea ice, as observed by Maykut and McPhee, 1995, McPhee et al, 2003 and Perovich et al, 2008. Hence the surface energy balance in the Arctic Ocean is of primary importance in controlling the evolution of sea ice volume.

The surface energy balance is composed of four radiative fluxes (downwelling and upwelling SW and LW), two turbulent fluxes (sensible and latent) and of an additional flux due to snowfall. The radiative fluxes dominate in terms of magnitude in both observations (e.g. Persson et al, 2002) and models (the relative magnitude of radiative and turbulent fluxes in HadGEM2-ES is demonstrated in Figure 2). For this reason, and because no large-scale observations of the turbulent fluxes or snowfall exist, in this study we analyse processes affecting only the radiative fluxes.

We express the net radiative flux $F_{SW} + F_{LW}$, where F_{SW} and F_{LW} are fluxes of net surface SW and LW radiation respectively, as functions of key Arctic climate variables using two formulae derived in Appendix A, valid for the ice freezing and melting seasons respectively (as different processes are important depending on the season). The formulae are applied to monthly means of data in model grid cells measuring tens of km across, within which the relevant variables are not necessarily constant or uniform; errors associated with this spatial and temporal extrapolation are briefly discussed in Appendix B.

During the ice freezing season

$$F_{SW} + F_{LW} = \frac{\alpha_{ice} F_{SW\downarrow} + F_{LW\downarrow} + C + BT_b}{1 - B \cdot R_{ice}} \qquad (1)$$

where $F_{SW\downarrow}$ and $F_{LW\downarrow}$ are fluxes of downwelling SW and LW radiation respectively, $R_{ice} = \frac{h_I}{k_I} + \frac{h_s}{k_s}$ is the thermal insulance of the ice and snow column (k_I and k_s being ice and snow conductivity respectively, h_I and h_S ice and snow thickness), B is the linearised rate of upwelling longwave dependence on surface temperature at 0°C, T_b ice base temperature in Celsius, C upwelling longwave at 0°C and α_I ice albedo.

During the ice melting season

$$F_{SW} + F_{LW} = F_{LW\downarrow} + C + F_{SW\downarrow} \bullet (1 - \alpha_{sea} - a_{ice}(\alpha_{ice} - \alpha_{sea}) - a_{snow}(\alpha_{snow} - \alpha_{ice}) - a_{cold}(\alpha_{cold} - \alpha_{snow}))$$

(2).

The Cryosphere Discuss., https://doi.org/10.5194/tc-2018-60
Manuscript under review for journal The Cryosphere
Discussion started: 6 April 2018

where α_{sea}, α_{snow} and α_{cold} indicate albedo of open sea, melting snow on sea ice and cold snow on sea ice respectively; a_{snow} and a_{cold} indicate the corresponding area fractions.

(1) and (2) summarises the dependence of surface radiative flux, assumed to account for the major part of the surface flux, on ice thickness, snow thickness, downwelling longwave and shortwave fluxes, ice fraction, snow fraction and melting surface fraction, during the freezing and melting seasons respectively. Hence, at each point in space and time, if a model bias in one of these quantities is known, an associated surface flux anomaly can be estimated to first order by multiplying the bias in the quantity by the partial derivative of (1) or (2) with respect to that quantity, calculated at some reference state. For example, given a model anomaly in ice thickness $\left(h_I^{MODEL} - h_I^{OBS}\right)$ during the freezing season, a resulting induced surface flux anomaly can be calculated as

$$\left[\Delta F_{sfc}\right]_{h_I} \approx \left(h_I^{MODEL} - h_I^{OBS}\right) \bullet \frac{\partial F_{sfc}}{\partial h_I} = \left(h_I^{OBS} - h_I^{MODEL}\right) \bullet \frac{B}{k_I} \cdot \frac{LW_{down}^{REFERENCE} + BT_b}{\left(1 - Bh_{I\_eff}^{REFERENCE}\right)^2} \qquad (3)$$

(Here the SW flux is neglected for clarity).

In a similar way, given a model anomaly of melting surface fraction for any point in space and time, an induced surface flux anomaly can be calculated in a similar way to above, by multiplying the model anomaly in melt onset occurrence by the partial derivative of (7) with respect to melt onset occurrence:

$$\left[\Delta F_{sfc}\right]_{melt\_onset} = \left(I_{cold}^{MODEL} - I_{cold}^{OBS}\right) \bullet SW_{down}^{REFERENCE}\left(\alpha_{cold} - \alpha_{snow}\right) \qquad (4)$$

Using equations (1) and (2), an induced surface flux anomaly due to downwelling SW, downwelling LW, ice thickness, ice fraction and melt onset occurrence was calculated for all model grid cells, for all months in the period 1980-1999. Firstly, a model anomaly in the relevant climate variable was calculated by bilinearly regridding the chosen observational dataset to the model grid, and then averaging this across all dataset years into a climatology. The model bias in the relevant quantity for each grid cell and model month was then calculated by subtracting this climatology. Secondly, to convert the modelled bias in the relevant quantity to an induced surface flux anomaly, the fields were multiplied by the partial derivative of equation (1) (where modelled $T_{sfc} < -1°C$) or equation (2) (where $T_{sfc} \geq -1°C$). Where observational datasets were available, the reference quantities in the partial derivative fields were calculated as model-observation means. Where no such datasets were available (e.g. for snow thickness), the model field was used. No flux anomalies due to snow thickness or snow fraction were computed, due to a lack of observational datasets with which to calculate model anomaly in these quantities.

3. Evaluating sea ice and surface radiation in HadGEM2-ES

From 1980-1999, the four members of the HadGEM2-ES historically-forced ensemble simulate a mean September sea ice extent of 5.78 x 10^6 km^2, with ensemble standard deviation of 0.24 x 10^6 km^2. By comparison, the mean observed September sea ice extent over this period was 6.88 x 10^6 km^2 according to the

HadISST1.2 dataset. Over the reference period, therefore, modelled September sea ice extent is systematically lower than that observed (Figure 3a).

Mean ice thickness is consistently lower than that estimated by PIOMAS for the Arctic Ocean region (Figure 3b), with the highest anomalies of -0.4m occurring in October, close to the minimum of the annual cycle, and a near-zero anomaly in May, close to the maximum. Modelled ice thickness is also biased low relative to Envisat (Figure 3c), with thickness anomalies ranging from -1.06m in November to -0.72m in April, and relative to the submarine data (Figure 3d), with thickness anomalies ranging from -1.5m in August to -0.8m in January and May. Hence it is very likely that ice thickness in HadGEM2-ES is biased low in the annual mean, with anomalies tending to be higher when ice thickness is lower. In other words, the ice thickness annual cycle of HadGEM2-ES is likely to be too amplified, with both anomalously high ice melt during the summer and ice growth during the winter.

Maps of the ice thickness bias in April and October (Figure 3b-d) show agreement that the low ice thickness bias is smaller on the Pacific side of the Arctic than on the Atlantic side of the Arctic, becoming very small or even positive in the Beaufort Sea. There is also striking agreement in the spatial pattern of the amplification bias of the seasonal cycle, as diagnosed by April-October ice thickness difference (Figure 4). All three ice thickness datasets show the HadGEM2-ES ice thickness seasonal cycle to be too amplified across much of the Arctic, by up to 1m in the Siberian shelf seas; in addition, all show that in the Beaufort Sea, the amplification is nonexistent or even negative. There is clear association between areas where modelled annual mean ice thickness is biased low, and areas where the modelled seasonal cycle is overamplified, and vice versa.

In the following discussion of radiative fluxes, the convention is that positive numbers denote a downwards flux. Fluxes of downwelling SW radiation are higher in HadGEM2-ES than in all observational estimates during the spring (Figure 5a-c), with May anomalies of 26, 41 and 53 Wm^{-2} relative to CERES, ERAI, and ISCCP-FD respectively. We note that as ERAI and ISCCP-FD have been found to underestimate downwelling SW during spring at specific locations, the true model anomaly is perhaps more likely to lie towards the lower end of these estimates. During the summer, upwelling SW radiation is consistently lower in magnitude HadGEM2-ES, with June anomalies of 14, 33 and 40 Wm^{-2} with respect to ERAI, CERES and ISCCP-FD respectively (a positive anomaly in an upward flux demonstrates that the model is too low in magnitude). There is no consistent signal for a low bias in downwelling SW during the summer, suggesting a model surface albedo bias. The effect is that modelled net downward SW flux is too large with respect to all observational datasets in May and June, and with respect to some in July and August. Relative to CERES, the May downwelling SW bias displays no clear spatial differentiation over the Arctic Ocean (Figure 5a), but the June upwelling SW bias, and hence the net SW bias, tend to be somewhat higher in magnitude towards the central Arctic (Figure 5b-c).

Fluxes of longwave (LW) radiation are lower in magnitude in HadGEM2-ES throughout the winter than in all observational datasets (Figure 5d-f). For downwelling LW, the mean model anomalies from December-April are -15, -22 and -27 Wm^{-2} for ERAI, CERES and ISCCP-FD respectively; for upwelling LW, the anomalies are 11, 15 and 16 Wm^{-2} for CERES, ERAI and ISCCP respectively. Because the downwelling LW anomalies vary more than the upwelling LW anomalies, there is uncertainty in inferring a model bias in net downwelling LW; ISCCP suggests a large model bias of -21 Wm^{-2}, CERES a smaller bias of -11 Wm^{-2}, while ERAI suggests no bias at

The Cryosphere Discuss., https://doi.org/10.5194/tc-2018-60
Manuscript under review for journal The Cryosphere
Discussion started: 6 April 2018

all. As in situ studies have shown both underestimation (by CERES) and overestimation (by ERAI and ISCCP-FD) of downwelling LW in winter, there is no clear indication as to where the true model anomaly in this quantity may lie. Maps of the downwelling and net down LW bias relative to CERES in February (Figure 5d,f) show the bias tends to be somewhat higher towards the North American side of the Arctic, and lower on the Siberian side.

In summary, there is evidence of a low bias in net downward LW during the winter, and a high bias in net downward SW during the summer, each of order of magnitude ~10 Wm^{-2}. This is consistent with surface radiation fluxes being the likely first-order cause of the amplified sea ice thickness seasonal cycle. In the next section we attempt to attribute the surface radiation biases to particular processes using the methodology described in Section 2.

4. Induced surface flux anomaly

We calculate fields of surface flux anomaly for each month in the model period 1980-1999 induced by model anomalies in downwelling LW, downwelling SW, ice thickness, ice fraction and melt onset occurrence, using in turn CERES, ISCCP-FD and ERAI as reference datasets. The resulting fields are integrated over the Arctic Ocean and averaged over the model period 1980-1999 to produce, for each climate variable, a seasonal cycle of average induced surface flux anomaly. In Figure 6, the seasonal cycles of each component of the surface flux anomaly are shown as a set of stacked barplots, with the results using CERES, ISCCP-FD and ERAI as reference shown from left-right for each month. These are compared, firstly to the net radiative flux anomalies implied by the direct radiation evaluation above (using again CERES, ISCCP-FD and ERAI in turn), and secondly to the sea ice latent heat flux uptake anomaly implied by the ice volume anomalies relative to PIOMAS.

Consistent with the direct radiation comparison and the ice volume anomalies, the induced surface flux anomalies usually sum to positive values during the summer and negative values during the winter. This implies that model biases in the processes investigated tend to cause anomalous ice melt during the summer and anomalous ice growth during the winter. Despite the large discrepancies between the radiative flux estimates of CERES, ISCCP-FD and ERAI, the choice of radiation dataset does not significantly affect any of the induced surface flux anomalies save those due to downwelling SW and LW radiation in the summer, where very large spread is apparent.

Induced surface flux anomalies are generally small in May. In June an anomaly of 8 Wm^{-2} is induced by melt onset occurrence; the SSMR observations do not show melt onset to occur in the central Arctic until late June on average, while HadGEM2-ES allows the entire Arctic Ocean to reach the melting temperature by the end of May, inducing a large model anomaly in surface albedo. June also displays a small but growing surface flux anomaly due to ice fraction anomaly, consistent with the anomalously fast ice melt of HadGEM2-ES. By August, although there is no remaining melt onset occurrence anomaly, the surface flux anomaly due to ice fraction is 9-10 Wm-2, allowing the positive surface flux anomaly to be maintained throughout the summer.

As noted above, the surface flux anomaly due to downwelling SW and LW radiation varies greatly with the use of observational dataset throughout the summer. Existing in situ validation studies of ERAI (Lindsay et al, 2014) and of CERES (Christensen et al, 2016) show both datasets to model downwelling LW accurately to within 15 Wm-2, although CERES is shown to be biased high in June and low in August, while ERAI is biased high in July. Even if these results were representative of the broader Arctic Ocean, it would be hard to interpret the true net effect of the combined LW and SW anomalies, as these will tend to be opposite in sign and of similar orders of magnitude. It is concluded that it is not possible to determine the net effect of downwelling radiative anomalies on surface flux during the summer with current observational data.

As the surface of the Arctic Ocean begins to cool in early autumn, a growing negative anomaly due to the now large deficit in ice thickness begins to appear, reaching a maximum of -6 Wm^{-2} in November. The anomaly reduces sharply through the winter as model anomalies in ice thickness with respect to PIOMAS become smaller. From November – April, the downwelling LW induces an additional negative surface flux anomaly, with a mean value of -4 Wm^{-2} indicated from December – February. It is superficially surprising that the choice of radiation dataset does not greatly affect the total induced surface flux, given the large spread in net LW radiation during winter estimated by each dataset. This occurs because in the induced surface flux analysis, the upwelling LW flux anomaly is calculated from other variables, and is therefore strongly anti-correlated with the downwelling LW flux anomaly estimate via the surface temperature.

The sum of the induced surface flux anomalies is of a similar shape and order of magnitude to the sea ice latent heat anomalies implied by the thickness anomalies with respect to PIOMAS (Figure 6), with positive anomalies of order 10 Wm-2 during the ice melt season, and negative anomalies of order 5 Wm-2 during the ice freeze season. The most obvious discrepancy occurs in July, when the sum of the induced surface flux anomalies is small and of indeterminate sign, while a large positive anomaly is implied by the sea ice thickness simulation. This may be due to the 'missing process' of surface albedo anomaly due to the presence of snow on sea ice. Early surface melt onset, and sea ice fraction loss, as modelled by HadGEM2-ES, would be expected to be associated also with early loss of snow on sea ice, with an associated surface albedo anomaly, with this process reaching its maximum influence at a time between that of the surface melt onset (June) and that of the sea ice fraction loss (August).

In winter the sum of the induced anomalies is consistently lower in magnitude than the sea ice latent heat flux anomaly, indicating that the tendency of model anomalies ice thickness and downwelling LW to cause additional ice growth does not fully account for the anomalous growth seen relative to PIOMAS . This may be due to the use of ice thickness reference dataset; it was noted in Section 2.3 that PIOMAS may underestimate ice thickness in late winter, which would cause the sea ice latent heat flux anomaly, and the surface flux anomaly induced by ice thickness anomalies, to be overestimated and underestimated respectively. It may also indicate that model anomaly in snow thickness, not investigated here, plays a part in inducing additional surface flux anomaly. A third factor in play may be sub-gridscale variation in ice thickness, which as discussed in Appendix B causes an underestimate in the freezing season surface flux anomalies of the order of 10%, or ~1 Wm^{-2}. It is noted that errors due to sub-monthly scale time covariance in the relevant climate variables, discussed further in Appendix B, are an order of magnitude lower than most absolute values discussed here, and in the context of the large observational uncertainties are unlikely to be important.

The Cryosphere Discuss., https://doi.org/10.5194/tc-2018-60
Manuscript under review for journal The Cryosphere
Discussion started: 6 April 2018

Consistent with the pattern of net SW anomaly identified in section 3, the spatial pattern of surface flux anomaly induced by melt onset occurrence is characterised by a weak maximum in the central Arctic, with values falling away towards the coast. A more sharply-defined pattern is produced by the ice fraction anomaly in August, with high values across the shelf seas and the Atlantic side of the Arctic falling to low or negative values in the Beaufort Sea; the pattern displayed by the ice thickness-induced anomaly in November is almost a mirror image. Finally, the surface flux anomaly induced by downwelling LW in February displays slightly higher values on the Siberian side of the Arctic than the American side, the reverse pattern to that displayed by the downwelling LW itself in Figure 5d. The contrast is due to the role the effective ice thickness scale factor plays in determining the induced surface flux anomaly; thicker ice, such as that which tends to be found on the American side of the Arctic in both model and observations, tends to greatly reduce the flux anomaly. This represents the thickness-growth feedback, the reality that thicker ice will grow less quickly than thin ice under the same atmospheric conditions.

The surface flux anomalies produced by ice fraction anomalies in August, and ice thickness anomalies in November, provide reasons for the spatial variation in amplification of the ice thickness seasonal cycle seen in Figure 4, as well as the close resemblance of this pattern to the model anomalies in annual mean ice thickness. Ice which is thinner in the annual mean will tend to melt faster in summer, due to the net SW anomalies associated with greater creation of open water (the ice albedo feedback), and to freeze faster in winter, due to greater conduction of energy through the ice (the ice thickness-growth feedback).

5. Discussion

The calculation of the surface radiative flux anomalies induced by various key processes in the Arctic Ocean produces results qualitatively consistent with the surface radiation evaluation, and with the surface flux anomalies implied by the sea ice simulation. Melt onset occurrence and sea ice fraction anomalies tend to cause anomalous surface warming, and sea ice melt, during the summer; downwelling LW and ice thickness anomalies tend to cause anomalous surface cooling, and hence sea ice growth, during the winter. It is recognised that it would not be expected that the induced surface fluxes would sum to values exactly consistent with either the radiation evaluation, or the sea ice volume evaluation, due in the main to observational inaccuracy, but also due to the approximations made when deriving the simple models of Section 2.3.

It is helpful to divide the processes examined into feedbacks (surface flux anomalies induced by anomalies in the sea ice state itself) and forcings (those induced by downwelling radiative fluxes and melt onset occurrence).The surface flux anomaly induced by anomalies in ice fraction can be identified with the surface albedo feedback; that induced by anomalies in ice thickness can be identified with the thickness-growth feedback. The other processes examined – downwelling SW, LW and melt onset occurrence – can be viewed as external forcings. Demonstrated in Figure 7, the anomalous summer sea ice melt is initiated by the early melt onset occurrence, and maintained by the surface albedo feedback, which acts preferentially in areas of thinner ice; the anomalous winter ice growth is maintained both by the thickness-growth feedback (occurring mainly in areas of thinner ice, of greater importance in early winter) and by the downwelling LW anomaly (more spatially uniform, in late winter). It is unclear that any significant role is played by the downwelling SW anomaly, as at

the only time of year when the radiation datasets agree that this anomaly is of significant value (May), the induced surface flux anomaly is more than balanced by that induced by downwelling LW. However this may have a role in causing the later melt onset anomaly, as discussed below.

The means by which the external forcings – anomalous LW winter cooling, and early late spring melt onset – cause an amplified seasonal cycle in sea ice thickness are clear. It is also possible to understand how, in the absence of other forcings, these combine to create an annual mean sea ice thickness which is biased low, as seen in Section 3. The melt onset forcing, by inducing additional ice melting through its effect on the ice albedo, acts to greatly enhance subsequent sea ice melt through the surface albedo feedback. The downwelling LW, on the other hand, by inducing ice freezing, acts to attenuate subsequent sea ice freezing through the thickness-growth feedback. The effect is that surface flux anomalies induced by melt onset occurrence are enhanced, while those induced by downwelling LW are diminished.

Acting together, the ice thickness-growth feedback and surface albedo feedback create a strong association between lower ice thicknesses and amplified seasonal cycles, because ice which tends to be thinner will both grow faster during the winter, and melt faster during the summer. Hence the melt onset anomaly, acting alone, would induce a seasonal cycle of sea ice thickness both lower, and more amplified, than that observed, while the downwelling LW anomaly acting alone would induce a seasonal cycle of ice thickness higher and less amplified. The bias seen in HadGEM2-ES is a result of the melt onset anomaly 'winning out' over the downwelling LW, due to its occurring at a time of year when the intrinsic sea ice feedbacks render the ice far more sensitive to surface radiation. The anomalously low ice cover in September arises as a consequence of the low annual mean ice thickness, and in particular of the anomalously severe summer ice melt.

The feedbacks of the sea ice state explain the association between spatial patterns of annual mean ice thickness bias and ice thickness seasonal cycle amplification. However, the external forcings (melt onset and downwelling LW bias) cannot entirely explain the spatial patterns in the mean sea ice state biases, because on a regional scale effects of sea ice convergence, and hence dynamics, become more important. The annual mean ice thickness bias seen in HadGEM2-ES is associated with a thickness maximum on the Pacific side of the Arctic, at variance with observations which show a similar maximum on the Atlantic side. It was shown by Tsamados et al (2013) that such a bias could be reduced by introducing a more realistic sea ice rheology.

The study would be incomplete without a discussion of possible causes of the two external drivers identified by this analysis as causing sea ice model biases. Underestimation of wintertime downwelling LW fluxes is known to be a widespread model bias in the CMIP5 ensemble (e.g. Boeke and Taylor, 2016). Pithan et al (2014) showed that this bias was likely to be a result of insufficient liquid water content of clouds forming in subzero air masses, resulting in a failure to simulate a particular mode of Arctic winter climate over sea ice; the 'mild mode', characterised by mild surface temperatures and weak inversions, whose key diagnostic is observed to be a net LW flux of close to 0 Wm^{-2} (Stramler et al, 2011; Raddatz et al, 2015 amongst others). HadGEM2-ES was not one of the models assessed by Pithan et al (2014), but its winter climate simulation displays many of the characteristic biases displayed by these, notably a tendency to model very low cloud liquid water fractions during winter compared to MODIS observations (Figure 8a) and a failure to simulate the milder mode of Arctic winter climate as demonstrated in SHEBA observations, diagnosed by 6-hourly fluxes of net LW (Figure 8b).

Here we concludethat a similar mechanism is likely to be at work in HadGEM2-ES, and that insufficient cloud liquid water is the principal driver of the anomalously low downwelling LW fluxes.

The causes of the early melt onset bias of HadGEM2-ES are harder to determine. For most of the spring, comparison of daily upwelling LW fields of HadGEM2-ES to CERES-SYN observations (not shown) shows the Arctic surface to be anomalously cold in the model, as during the winter. During May, however, upwelling LW values rise much more steeply in the model, and surface melt onset commences during mid-to-late May, far earlier than in the satellite observations. A possible cause of the overly rapid surface warming during May is the zero-layer thermodynamics approximation used by HadGEM2-ES, in which the ice heat capacity is ignored. Comparing fields of surface temperature in HadGEM2-ES between the beginning and the end of May shows a 'missing' ice sensible heat uptake flux of 10-30 Wm-2 over much of the central Arctic, which would in turn be associated with a reduction of flux into the upper ice surface of 5-15 Wm-2. Examination of modelled and observed daily timeseries of downwelling LW and net SW fluxes in late May and early June suggests that a surface flux reduction of this magnitude could delay surface melt by up to 2 weeks, a substantial part of the modelled melt onset anomaly seen.

Another cause of the rapid warming may be the increasing relative magnitude of the downwelling SW response to cloud anomalies as May progresses (compared to the downwelling LW response). Comparison of 5-daily means of HadGEM2-ES radiative fluxes during May to those from the CERES-SYN product (not shown) support this hypothesis; a modelled anomaly in downwelling SW grows quickly during early May, from ~ $0Wm^{-2}$ to ~ $30Wm^{-2}$, while the modelled anomaly in downwelling LW remains roughly constant.

6. Conclusions

HadGEM2-ES simulates a sea ice cover which is not extensive enough at annual minimum. Comparison to various ice thickness datasets shows that it also has too low an annual mean ice thickness, and that its ice thickness seasonal cycle is likely to be overamplified. Evidence of a positive net SW bias during the ice melt season, and a negative net LW bias during the ice freezing season is apparent from evaluations using multiple radiation datasets.

An evaluation of processes influencing surface radiation, combined with simple models to estimate their effect, produces results consistent with the evaluation of the sea ice state and surface radiation; processes tend to cause anomalous ice melt during the melting season, and anomalous ice growth during the freezing season. Consequently model anomalies in sea ice growth and melt rate can be attributed in detail to different causes; in particular, the roles played by the sea ice albedo feedback, by the sea ice thickness-growth feedback, and by external forcings, can be quantified. The analysis reveals how the melt onset anomaly of HadGEM2-ES tends to make model ice thickness both low in the annual mean, and too amplified in the seasonal cycle, with the downwelling LW anomaly acting to mitigate both effects. The result is consistent with the prediction of DeWeaver et al (2008) that sea ice state is more sensitive to surface forcing during the ice melt season than during the ice freeze season. The analysis also suggests that through an indirect effect on surface albedo at a time when sea ice is particularly sensitive to surface radiation anomalies, the zero-layer approximation, which

was until recently commonplace in coupled models, may be of first-order importance in the sea ice state bias of HadGEM2-ES.

The analysis also makes explicit the link between the spatial pattern of anomalies in annual mean ice thickness, and anomalies in the April-October ice thickness difference. Regions where ice thickness tends to be biased particularly low in the annual mean also display higher amplification in the seasonal cycle, due to the direct action of the thickness-growth and ice albedo feedbacks, despite the initiating factors of melt onset occurrence and downwelling LW anomaly being comparatively spatially uniform. However, the reasons for the underlying spatial distribution of the annual mean ice thickness anomalies in HadGEM2-ES are likely to lie in ice dynamics rather than thermodynamics.

The method is limited by the current inability to evaluate the impact of anomalies in modelled snow cover, as well as by the large observational uncertainties in summer surface radiation, underlying the importance of reducing uncertainty in large-scale observations of Arctic climate variables. Adding in the 'missing processes' of freezing season snow thickness, and melt season snow fraction, would represent useful extensions to the analysis presented. Other potential causes of SEB anomalies not investigated in this study include processes causing anomalies in the turbulent fluxes, and in particular the effects of anomalies in sea ice fraction during the freezing season.

In the case study presented here, the analysis provides mechanisms behind a model bias in sea ice simulation. However, the analysis could also be used to investigate a sea ice simulation that was ostensibly more consistent with observations, to determine whether or not the correct simulation was the consequence of model biases that cause opposite errors in the surface energy budget; a negative result would greatly increase confidence in the future projections of such a model. The analysis could be also used to investigate a whole model ensemble, to attribute spread in modelled sea ice state to spread in the underlying processes affecting the SEB, focussing attention on ways in which spread in modelled sea ice could be reduced. It is noteworthy that Shu et al (2015) found the CMIP5 ensemble mean Arctic sea ice volume to be biased low in the annual mean, and overamplified in the seasonal cycle, relative to PIOMAS (albeit over the entire Northern Hemisphere), suggesting that the behaviour exhibited by HadGEM2-ES may be quite common in this ensemble.

Appendix A: Derivation of formulae used for surface flux analysis

The surface energy balance equation over an area of sea ice and open water, in which fluxes arriving at the surface from above are equated with fluxes of energy into the ice and ocean below, can be expressed as follows, ignoring the contribution from snowfall occurring on both sides:

$$F_{SW} + F_{LW} + F_{sens} + F_{lat} = F_{cond} + F_{melt} + F_{sublim} + F_{wat} \qquad \text{(A1)}$$

Here F_{SW}, F_{LW}, F_{sens}, F_{lat}, F_{cond}, F_{melt}, F_{sublim} and F_{wat} refer to fluxes of net SW, LW, sensible and latent heat flux, conductive heat flux into sea ice, top melting flux into sea ice, sea ice net sublimation flux, and flux of energy directly into seawater. Here and below, the convention used is that positive numbers denote

The Cryosphere Discuss., https://doi.org/10.5194/tc-2018-60
Manuscript under review for journal The Cryosphere
Discussion started: 6 April 2018

downward fluxes. For the reasons given above, we neglect the turbulent heat fluxes. By implication we also neglect the sea ice net sublimation flux. Hence the surface flux is equated with $F_{SW} + F_{LW}$.

During the ice freezing season, surface temperatures are below freezing, conduction into the ice is substantial, and $F_{melt} = 0$. In addition, ice fraction tends to be close to 1 over much of the Arctic. We assume for the purposes of this analysis that ice fraction during the freezing season is equal to 1 (equivalent to neglecting F_{wat}), while recognising that due to turbulent fluxes being observed to be very large in regions of open water, F_{wat} may in reality be of significant size. In the following analysis, as a result, the effects of model anomalies in ice fraction during the freezing season on the surface flux are not estimated.

Linearising the dependence of $F_{SW} + F_{LW}$ on the surface temperature T_{sfc} about the freezing point as $A + BT_{sfc}$, and assuming uniform conduction within the ice (thereby ignoring sensible heating of ice), we have

$$A + BT_{sfc} = \frac{T_{sfc} - T_b}{R_{ice}} \qquad \text{(A2)}$$

where the ice thermal insulance $R_{ice} = h_I / k_I + h_S / k_S$, h_I, h_S, k_I and k_S being ice and snow thickness, and ice and snow conductivity, respectively.

Solving for T_{sfc} and re-substituting, we have

$$F_{SW} + F_{LW} = \frac{A + BT_b}{1 - B \cdot R_{ice}} \qquad \text{(A3)}$$

A represents the surface temperature-independent part of the surface flux, and can be identified with $F_{SW} + F_{LW\downarrow} + C$, where $F_{LW\downarrow}$ is the downwelling LW flux and *C* is the upwelling longwave flux associated with a surface temperature of 0°C. Hence

$$F_{sfc} = \frac{\alpha_I F_{SW\downarrow} + F_{LW\downarrow} + C + BT_b}{1 - B \cdot R_{ice}} \qquad \text{(A4)}$$

Equation (A4) summarises the dependence of the net radiative flux on downwelling radiative fluxes and on ice and snow thickness, and is equivalent to equation (1), used to calculate induced surface flux anomaly during the freezing season.

During the ice melting season, conductive flux is near zero, surface temperature is close to 0°C throughout, and ice fraction is no longer necessarily close to 1. Hence the surface flux is

$$F_{sfc} = F_{LW\downarrow} + C + \alpha_S F_{SW\downarrow} \qquad \text{(A5)}$$

where α_S is surface albedo and $C = \varepsilon\sigma T_f^4$ is upwelling longwave radiation at $T_f = 0°C$. In HadGEM2-ES, surface albedo is parameterised after Curry et al (2001), which approximates the effect of sea ice meltponds by reducing albedo as the surface temperature approaches the melting point. Surface albedo is therefore affected by ice fraction, the presence or otherwise of snow, and whether or not melt onset has occurred. The effect can be summarised as

$$F_{sfc} = F_{LW\downarrow} + C + F_{SW\downarrow} \bullet (1 - \alpha_{sea} - I_{ice}(\alpha_{ice} - \alpha_{sea}) - I_{snow}(\alpha_{snow} - \alpha_{ice}) - I_{cold}(\alpha_{cold} - \alpha_{snow})) \quad \text{(A6)}.$$

where α_{sea}, α_{ice}, α_{snow} and α_{cold} indicate the modelled albedos of open water, bare ice, melting snow and cold snow respectively, and I_{ice}, I_{snow} and I_{cold} indicate the presence of sea ice, snow cover and cold snow (that is far from the melting point) respectively. Integrated over large areas, I_{ice} becomes ice area fraction a_{ice} (and similarly for I_{snow} and I_{cold}), giving equation (2), used to calculate induced surface flux anomaly during the melting season.

Appendix B: Error associated with spatial and temporal extrapolation

The application of equations (A4) and (A6) to monthly means of data valid for grid cells tens of km across introduces two potential sources of error in estimating the surface flux anomaly induced. Firstly, subgridscale variation in ice thickness, which is not accounted for by the simple model, tends to increase the efficiency of heat loss and hence ice creation during the freezing season via the scale factor $\frac{1}{1 - Bh_{I\_eff}}$, rendering ice growth more sensitive to errors in the forcing variable. In an analysis of a field of category ice thickness produced by HadGEM2-ES for January 1994, this was found to cause an average underestimate of 8% in the scale factor value, and hence the induced surface flux anomaly.

Secondly, error will occur due to covariance in time between variables being multiplied. As both melt onset occurrence and ice fraction observations were available on daily timescales, the effect of this covariance was assessed by calculating induced surface flux anomaly due to melt onset occurrence and ice fraction on both daily and monthly timescales. The daily covariance was found to cause a maximum error of 0.1 Wm^{-2} in the melt onset-induced anomaly, in June, and of 0.5 Wm^{-2} in the ice fraction-induced anomaly, in August, with most other monthly anomalies being below 0.1 Wm^{-2}.

Code availability

The code used to create Figures 1-8 is written in Python and is provided as a supplement (directory 'Figures'). In addition, the routine used to create the monthly induced surface flux anomaly fields used in Figures 6&7 from

the basic model and observation fields is provided (directory 'Analysis'). A set of auxiliary routines used by most of the above are also provided (directory 'Library'). Most routines make use of the open source Iris library, and several make use of the open source Cartopy library.

Data availability

Monthly mean ice thickness, ice fraction, snow thickness and surface radiation, as well as daily surface temperature and surface radiation, for the first historical member of HadGEM2-ES, is available from the CMIP5 archive at https://cmip.llnl.gov/cmip5/data_portal.html.

NSIDC ice concentration and melt onset data can be downloaded at http://nsidc.org/data/NSIDC-0051 and http://nsidc.org/data/NSIDC-0105 respectively.

PIOMAS ice thickness data can be downloaded at http://psc.apl.uw.edu/research/projects/arctic-sea-ice-volume-anomaly/data/.

ERAI surface radiation data can be downloaded at http://apps.ecmwf.int/datasets/data/interim-full-daily/levtype=sfc/.

ISCCP-FD surface radiation data is available at https://isccp.giss.nasa.gov/projects/browse_fc.html.

CERES surface radiation data is available at https://climatedataguide.ucar.edu/climate-data/ceres-ebaf-clouds-and-earths-radiant-energy-systems-ceres-energy-balanced-and-filled.

Acknowledgements

This study was supported by the Joint UK BEIS/Defra Met Office Hadley Centre Climate Programme (GA01101).

Thanks are due to Richard Wood and Ann Keen for helpful comments on multiple versions of this study.

References

Anderson, M., Bliss, A. and Drobot, S.: Snow Melt Onset Over Arctic Sea Ice from SMMR and SSM/I-SSMIS Brightness Temperatures, Version 3. Boulder, Colorado USA. NASA National Snow and Ice Data Center Distributed Active Archive Center. doi: http://dx.doi.org/10.5067/22NFZL42RMUO [accessed October 2015], 2001, updated 2012

Bitz, C. M. and Roe, G. H.: A Mechanism for the High Rate of Sea Ice Thinning in the Arctic Ocean, J. Clim., 17, 18, 3623–3632, doi: https://doi.org/10.1175/1520-0442(2004)017, 2004

Bitz, C. M., Holland, M. M., Hunke, E. C., and Moritz, R. M.: Maintenance of the Sea-Ice Edge, J. Clim., 18, 15, 2903–2921, doi: https://doi.org/10.1175/JCLI3428.1, 2005

Bitz, C. M.: Some Aspects of Uncertainty in Predicting Sea Ice Thinning, in Arctic Sea Ice Decline: Observations, Projections, Mechanisms, and Implications (eds E. T. DeWeaver, C. M. Bitz and L.-B. Tremblay), American Geophysical Union, Washington, D.C.. doi: 10.1029/180GM06, 2008

Boeke, R. C. and Taylor, P. C.: Evaluation of the Arctic surface radiation budget in CMIP5 models, J. Geophys. Res. Atmos., 121, 8525-8548, doi:10.1002/2016JD025099, 2016

Christensen, M. W., Behrangi, A., L'ecuyer, T. S., Wood, N. B., Lebsock, M. D. and Stephens, G. L.: Arctic Observation and Reanalysis Integrated System: A New Data Product for Validation and Climate Study, B. Am. Meteorol. Soc., 97, 6, 907–916, doi: https://doi.org/10.1175/BAMS-D-14-00273.1, 2016

Collins, W. J., Bellouin, N., Doutriaux-Boucher, M., Gedney, N., Halloran, P., Hinton, T., Hughes, J., Jones, D., Joshi, M., Liddicoat, S., Martin, G., O'Connor, F., Rae, J., Senior, C., Sitch, S., Totterdell, I., Wiltshire, A. and Woodward, S.: Development and evaluation of an Earth-System model – HadGEM2. Geosci. Model Dev., 4, 1051-1075. doi:10.5194/gmd-4-1051-2011, 2011

Dee, D. P, Uppala, S. M., Simmons, A. J., Berrisford, P., Poli, P., Kobayashi, S., Andrae, U., Balmaseda, M. A., Balsamo, G., Bauer, P., Bechtold, P., Beljaars, A. C. M., van de Berg, L., Bidlot, J., Bormann, N., Belsol, C., Dragani, R., Fuentes, M., Geer, A., J., Haimberger, L., Healy, S. B., Hersbach, H., Holm, E. V., Isaksen, L., Kållberg, P., Köhler, M., Matricardi, M., McNally, A. P., Monge-Sanz, B. M., Morcrette, J.-J., Park, B.-K., Peubey, C., de Rosnay, P., Tavolato, C., Thépaut, J.-N. and Vitart, F.: The ERA-Interim reanalysis: configuration and performance of the data assimilation system. Quarterly Journal of the RMS 137:553:597. doi: 10.1002/qj.828, 2011

DeWeaver, E. T., Hunke, E. C. and Holland, M. M.: Sensitivity of Arctic Sea Ice Thickness to Intermodel Variations in the Surface Energy Budget. AGU Geophysical Monograph 180: Arctic Sea Ice Decline: Observations, Projections, Mechanisms and Implications, 77-91. doi: 10.1029/180GM07, 2008

Gultepe, I., Isaac, G. A., Williams, A., Marcotte, D. and Strawbridge, K. B., Turbulent heat fluxes over leads and polynyas, and their effects on arctic clouds during FIRE.ACE: Aircraft observations for April 1998, Atmosphere-Ocean, 41:1, 15-34, DOI: 10.3137/ao.410102, 2003

Hunke, E. C. and Dukowicz, J. K., An Elastic–Viscous–Plastic Model for Sea Ice Dynamics, J. Phys. Oceanogr., 27, 9, 1849–1867, doi: https://doi.org/10.1175/1520-0485(1997)027<1849:AEVPMF>2.0.CO;2, 1997.

Johns, T. C., Durman, C. F., Banks, H. T., Roberts, M. J., McLaren, A. J., Ridley, J. K., Senior, C. A., Williams, K. D., Jones, A., Rickard, G. J., Cusack, S., Ingram, W. J., Crucifix, M., Sexton, D. M. H., Joshi, M. M., Dong, B.-W., Spencer, H., Hill, R. S. R., Gregory, J. M., Keen, A. B., Pardaens, A. K., Lowe, J. A., Bodas-Salcedo, A., Stark, S. and Searl, Y.: The New Hadley Centre Climate Model (HadGEM1): Evaluation of Coupled Simulations. J Clim 19:1327-1353. doi: 10.1175/JCLI3712.1, 2006

Laxon, S., Peacock, N. and Smith, D.: High interannual variability of sea ice thickness in the Arctic region. Nature, 425, 947-950, doi:10.1038/nature02050, 2003

Laxon, S., Giles, K. A., Ridout, A., Wingham, D. J., Willatt, R., Cullen, R., Kwok, R., Schweiger, A., Zhang, J., Haas, C., Hendricks, S., Krishfield, R., Kurtz, N., Farrell, S. and Davidson, M.: Cryosat-2 estimates of Arctic sea ice thickness and volume. Geophys Res Lett 40:732-737. doi: 10.1002/grl.50193, 2013

Lindsay, R., Wensnahan, M., Schweiger, A. and Zhang, J.: Evaluation of Seven Difference Atmospheric Reanalysis Products in the Arctic, J. Clim., 27, 2588-2606, oi: 10.1175/JCLI-D-13-00014.1, 2013.

Lindsay, R. and Schweiger, A.: Arctic sea ice thickness loss determined using subsurface, aircraft, and satellite observations. The Cryosphere, 9, 269-283. doi: 10.5194/tc-9-269-2015, 2015

Lipscomb, W. H. and Hunke, E. C., Modeling Sea Ice Transport Using Incremental Remapping, Mon. Weather Rev., 132, 6, 1341–1354, doi: https://doi.org/10.1175/1520-0493(2004)132<1341:MSITUI>2.0.CO;2, 2004

Liu, J., J. A. Curry, Rossow, W. B., Key, J. R. and Wang, X.: Comparison of surface radiative flux data sets over the Arctic Ocean. J. Geophys. Res.: Oceans, 110, C2, doi: 10.1029/2004JC002381, 2005

Loeb, N. G., Wielicki, B. A., Doelling, D. R., Louis Smith, G., Keyes, D. F., Kato, S., Manalo-Smith, N. and Wong, T.: Toward Optimal Closure of the Earth's Top-of-Atmosphere Radiation Budget. J Cli, 22, 3, 748–766. doi: 10.1175/2008JCLI2637.1, 2009

Markus, T., Stroeve, J. C. and Miller, J.: Recent changes in Arctic sea ice melt onset, freezeup, and melt season length. J. Geophys. Res., 114, C12024. doi: 10.1029/2009JC005436, 2009

Martin, G. M., Bellouin, N., Collins, W. J., Culverwell, I. D., Halloran, P. R., Hardiman, S. C., Hinton, T. J., Jones, C. D., McDonald, R. E., McLaren, A. J., O'Connor, F. M., Roberts, M. J., Rodriguez, J. M., Woodward, S., Best, M. J., Brooks, M. E., Brown, A. R., Butchart, N., Dearden, C., Derbyshire, S. H., Dharssi, I., Doutriaux-Boucher, M., Edwards, J. M., Falloon, P. D., Gedney, N., Gray, L. J., Hewitt, H. T., Hobson, M., Huddleston, M. R., Hughes, J., Ineson, S., Ingram, W. J., James, P. M., Johns, T. C., Johnson, C. E., Jones, A., Jones, C. P., Joshi, M. M., Keen, A. B., Liddicoat, S., Lock, A. P., Maidens, A. V., Manners, J. C., Milton, S. F., Rae, J. G. L., Ridley, J. K., Sellar, A., Senior, C. A., Totterdell, I. J., Verhoef, A., Vidale, P. L. and Wiltshire, A., The HadGEM2 family of Met Office Unified Model climate configurations, Geosci. Model Dev., 4, 723-757, doi: https://doi.org/10.5194/gmd-4-723-2011, 2011

Maslanik, J., Stroeve, J. C., Fowler, C. and Emery, W.: Distribution and trends in Arctic sea ice age through spring 2011. Geophys. Res. Lett., 38, 47735. doi: 10.1029/2011GL047735, 2011

Massonnet, F., Fichefet, T., Goosse, H., Bitz, C. M., Philippon-Berthier, G., Holland, M. M. and Barriat, P.-Y.: Constraining projections of summer Arctic sea ice, The Cryosphere, 6, 1383–1394, doi: 10.5194/tc-6-1383-2012, 2012

Maykut, G. A. and McPhee, M. G., Solar heating of the Arctic mixed layer, J. Geophys. Res., 100, C12, 24,691-24,703, doi: 10.1029/95JC02554, 1995

McLaren, A. J., Banks, H. T., Durman, C. F., Gregory, J. M., Johns, T. C., Keen, A. B., Ridley, J. K., Roberts, M. J., Lipscomb, W. H., Connolley, W. M. and Laxon, S. W.: Evaluation of the sea ice simulation in a new coupled atmosphere-ocean climate model (HadGEM1). J. Geophys. Res., 111, C12014. doi: 10.1029/2005JC003033, 2006

McPhee, M. G., Kikuchi, T., Morison, J. H. and Stanton, T. P.: Ocean-to-ice heat flux at the North Pole environmental observatory, Geophys. Res. Lett., 30, 2274, doi:10.1029/2003GL018580, 2003

Notz, D.: How well must climate models agree with observations?. Philos T Roy Soc A, 373, 2052. doi: 10.1098/rsta.2014.0164, 2015

Perovich, D. K. and Elder, B., Estimates of ocean heat flux at SHEBA, Geophys. Res. Lett., 299, 9, 58-1 – 51-4, doi: 10.1029/2001GL014171, 2002

Perovich, D. K., Richter-Menge, J. A., Jones, K. F. and Light, B.: Sunlight, water, and ice: Extreme Arctic sea ice melt during the summer of 2007. Geophys. Res. Lett., 35, 11. doi: 10.1029/2008GL034007, 2008

Pithan, F., Medeiros, B. and Mauritsen, T.: Mixed-phase clouds cause climate model biases in Arctic wintertime temperature inversions, Clim. Dyn., 43, 289-303, doi:10.1007/s00382-013-1964-9, 2014

Raddatz, R. L., Papakyriakou, T. N., Else, B. G., Asplin, M. G., Candlish, L. M., Galley, R. J. and Barber, D. G.: Downwelling longwave radiation and atmospheric winter states in the western maritime Arctic. Int. J. Clim., 35, 9, 2339-2351. doi: 10.1002/joc.4149, 2014

Rayner, N. A., Parker, D. E., Horton, E. B., Folland, C. K., Alexander, L. V., Rowell, D. P., Kent, E. C. and Kaplan, A.: Global analyses of sea surface temperature, sea ice, and night marine air temperature since the late nineteenth century. J Geophys Res 108:4407. doi:10.1029/2002JD002670, 2003

Rothrock, D. A., Percival, D. B. and Wensnahan, M.: The decline in arctic sea ice thickness: Separating the spatial, annual, and interannual variability in a quarter century of submarine data. J. Geophys. Res., 113, C05003. doi: 10.1029/2007JC004252, 2008

Rutan, D. A., Kato, S., Doelling, D. R., Rose, F. G., Nguyen, L. T., Caldwell, T. E. and Loeb, N. G.: CERES Synoptic Product: Methodology and Validation of Surface Radiant Flux, J. Atmos. Ocean. Tech., 32(6), 1121-1143. http://dx.doi.org/10.1175/JTECH-D-14-00165.1, 2015

Schweiger, A. J.., Lindsay, R. W., Zhang, J., Steele, M. and Stern, H.: Uncertainty in modeled arctic sea ice volume, J. Geophys. Res., doi:10.1029/2011JC007084, 2011

Semtner, A. J.: A Model for the Thermodynamic Growth of Sea Ice in Numerical Investigations of Climate. J. Phys. Oceanogr., 6, 3, 379–389. doi: 10.1175/1520-0485, 1976.

Serreze, M. C., Barrett, A. P., Slater, A. G., Woodgate, R. A., Aagaard, K., Lammers, R. B., Steele. M., Moritz, R., Meredith, M. and Lee, C. M.: The large-scale freshwater cycle of the Arctic, J. Geophys. Res., 111, C11010, doi:10.1029/2005JC003424, 2006

Shu, Q., Song, Z. and Qiao, F. (2015) Assessment of sea ice simulation in the CMIP5 models. The Cryosphere, 9, 399–409. doi: 10.5194/tc-9-399-2015

Stramler, K., Del Genio, A. D. and Rossow, W. B.: Synoptically Driven Arctic Winter States. J. Clim., 24, 1747–1762. doi: 10.1175/2010JCLI3817.1, 2011

Stroeve, J. C., Kattsov, V, Barrett, A., Serreze, M., Pavlova, T., Holland, M. M. and Meier, W. N.: Trends in Arctic sea ice extent from CMIP5, CMIP3 and observations. Geophys. Res. Lett., 39, doi: 10.1029/2012GL052676, 2012a.

Stroeve, J. C., Serreze, M. C., Holland, M. M., Kay, J. E., Maslanik, J., Barratt, A. P.: The Arctic's rapidly shrinking sea ice cover: a research synthesis, Clim. Ch., 110, 1005–1027, doi: https://doi.org/10.1007/s10584-011-0101-1, 2012b

Swart, N. C., Fyfe, J. C., Hawkins, E., Kay, J. E. and Jahn, A.: Influence of internal variability on Arctic sea ice trends, Nat. Clim. Ch., 5, 86–89, doi:10.1038/nclimate2483, 2015

Thorndike, A. S., Rothrock, D. A., Maykut, G. A. and Colony, R., The thickness distribution of sea ice, J. Geophys. Res., 80, 4501-4513, doi: 10.1029/JC080i033p04501, 1975

Tsamados, M., Feltham, D. L. and Wilchinsky, A. V., Impact of a new anisotropic rheology on simulations of Arctic sea ice, J. Geophys. Res. – Oceans, 118, 1, 91-107, doi: 10.1029/2012JC007990, 2013

Wang, M. and Overland, J. E.: A sea ice free summer Arctic within 30 years? Geophys. Res. Lett., ., 36, L07502, doi:10.1029/2009GL037820, 2009

Wang, X., Key, J., Kwok, R. and Zhang, J.: Comparison of Arctic Sea Ice Thickness from Satellites, Aircraft and PIOMAS data, Remote Sens., *8*(9), 713; doi:10.3390/rs8090713, 2016

Zhang, Y., Rossow, W. B., Lacis, A. A., Oinas, V., and Mishchenko, M. I.: Calculation of radiative fluxes from the surface to top of atmosphere based on ISCCP and other global data sets: Refinements of the radiative transfer model and the input data, J. Geophys. Res., 109, D19105, doi:10.1029/2003JD004457, 2004

The Cryosphere Discuss., https://doi.org/10.5194/tc-2018-60
Manuscript under review for journal The Cryosphere
Discussion started: 6 April 2018

Figure 1. The Arctic Ocean region used in the analysis.

The Cryosphere Discuss., https://doi.org/10.5194/tc-2018-60
Manuscript under review for journal The Cryosphere
Discussion started: 6 April 2018

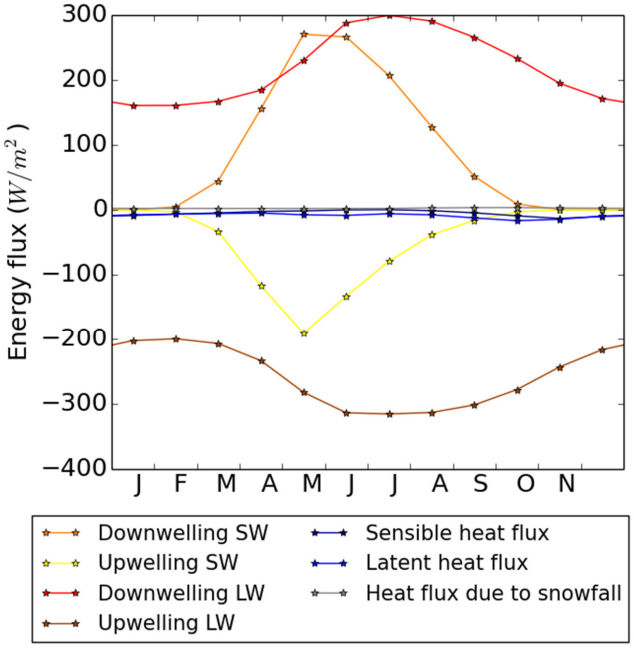

Figure 2. 1980-1999 mean surface fluxes over the Arctic Ocean region for the first historical run of HadGEM2-ES.

The Cryosphere Discuss., https://doi.org/10.5194/tc-2018-60
Manuscript under review for journal The Cryosphere
Discussion started: 6 April 2018

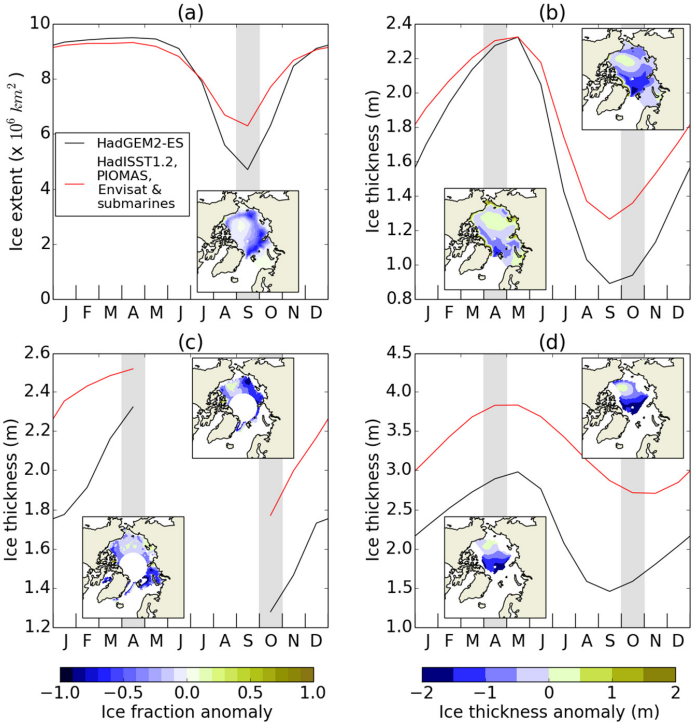

Figure 3. (a) HadGEM2-ES 1980-1999 mean Arctic Ocean ice extent, compared to HadISST1.2 1980-1999, with September ice fraction anomaly map; (b-d) HadGEM2-ES 1980-1999 ice thickness compared to (b) PIOMAS, (c) Envisat and (d) submarine datasets over respective regions of coverage, with April and October ice thickness anomaly maps. For each seasonal cycle plot, the model is in black and observations in red. In (c), data is not plotted from May-September due to the region of coverage being very small.

The Cryosphere Discuss., https://doi.org/10.5194/tc-2018-60
Manuscript under review for journal The Cryosphere
Discussion started: 6 April 2018

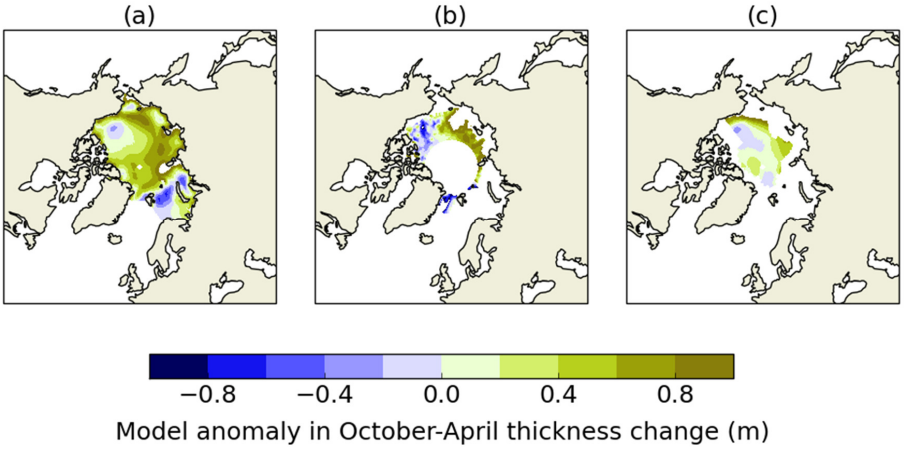

Figure 4. HadGEM2-ES 1980-1999 model anomaly in ice thickness change from October-April compared to (a) PIOMAS 1980-1999; (b) Envisat 1993-2000; (c) submarine regression analysis 1980-1999.

The Cryosphere Discuss., https://doi.org/10.5194/tc-2018-60
Manuscript under review for journal The Cryosphere
Discussion started: 6 April 2018

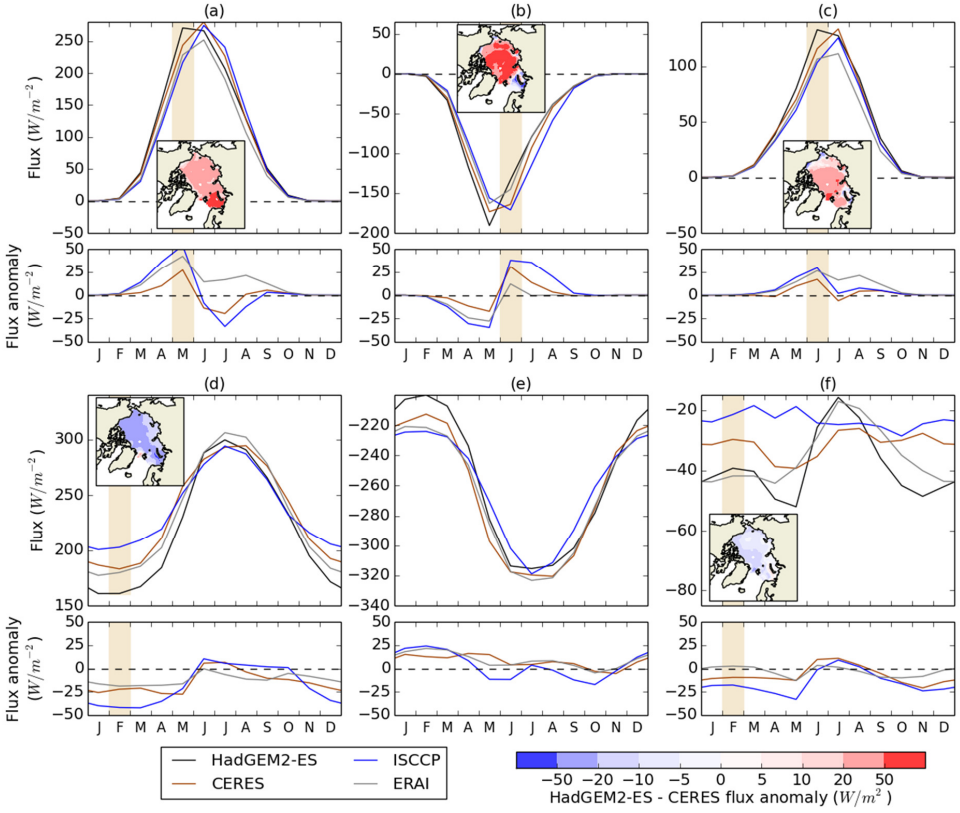

Figure 5. (a) Downwelling SW, (b) upwelling SW, (c) net down SW, (d) downwelling LW, (e) upwelling LW, (f) net down LW, for HadGEM2-ES 1980-1999 over the Arctic Ocean region, compared to CERES 2000-2013, ISCCP-D 1983-1999 and ERAI 1980-1999. For all fluxes, a positive number denotes a downward flux and vice versa. Maps of flux anomaly relative to CERES are shown for downwelling SW in May, upwelling and net down SW in June, and downwelling and net down LW in February.

The Cryosphere Discuss., https://doi.org/10.5194/tc-2018-60
Manuscript under review for journal The Cryosphere
Discussion started: 6 April 2018

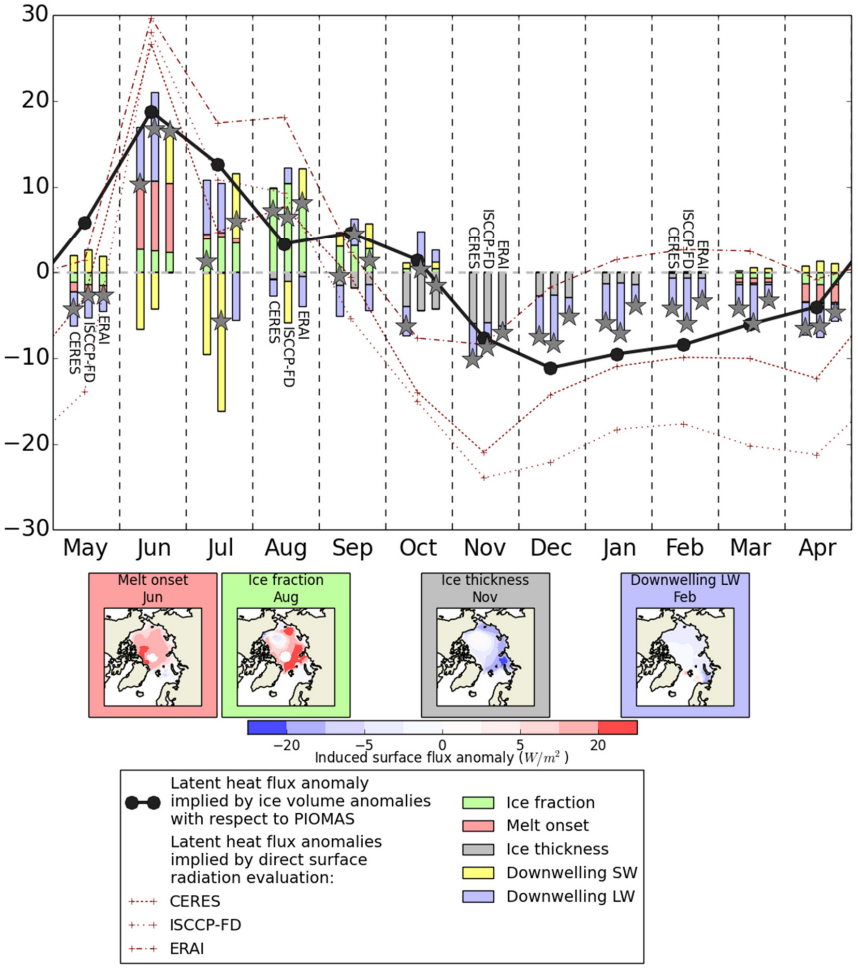

Figure 6. Surface flux anomaly induced by model anomalies in ice fraction, melt onset occurrence, ice thickness, downwelling SW and downwelling LW respectively, for the Arctic Ocean region in HadGEM2-ES, 1980-1999, as estimated by the simple models described in Section 2.3. For each month, induced anomalies are estimated using in turn CERES, ISCCP-FD and ERAI as radiation reference datasets, from left-right. Sea ice latent heat flux uptake anomaly relative to PIOMAS is indicated in black. Net radiative flux anomalies relative to CERES, ISCCP-FD and ERAI are indicated in brown. Spatial patterns of induced surface flux anomaly for four processes in key months, with CERES as reference dataset, are displayed beneath.

The Cryosphere Discuss., https://doi.org/10.5194/tc-2018-60
Manuscript under review for journal The Cryosphere
Discussion started: 6 April 2018

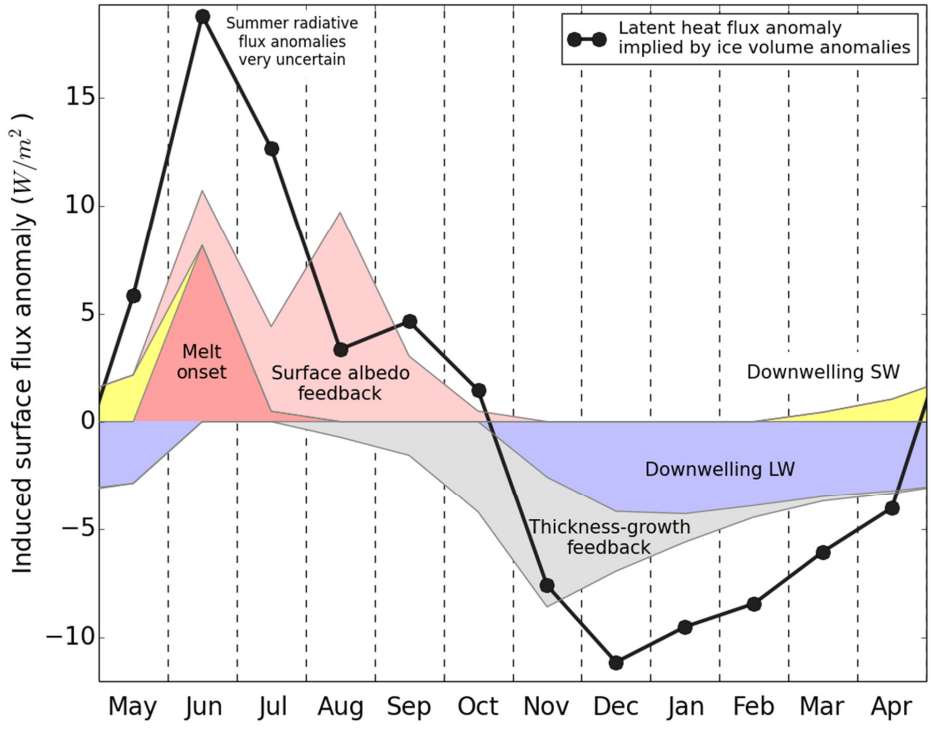

Figure 7. Surface flux anomalies caused by anomalies in external forcings, and to feedbacks due to anomalies in the sea ice state, represented as stacked filled regions. All values shown are means across radiation datasets shown in Figure 4; summer radiative flux anomalies are not plotted due to very large spread among datasets.

The Cryosphere Discuss., https://doi.org/10.5194/tc-2018-60
Manuscript under review for journal The Cryosphere
Discussion started: 6 April 2018

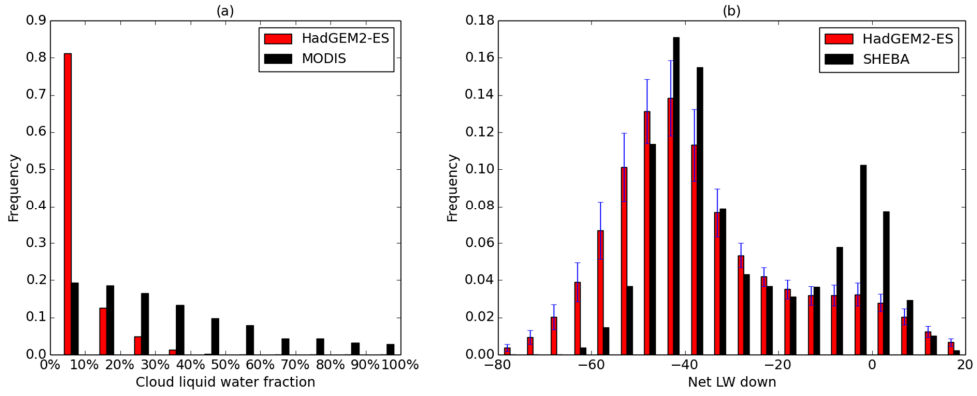

Figure 8. Frequency distributions of (a) October-April cloud liquid water percentage in HadGEM2-ES compared to MODIS observations, for the Arctic Ocean region; (b) December-February surface net downwelling LW in HadGEM2-ES in the SHEBA region, compared to the values observed at SHEBA.